ChemComm

Check for updates

Novel and more facile synthesis of highly dispersed iron in small-pore zeolites by ion exchange for catalytic applications†

Simon Barth, [ab] Leo Scheibe, [a] Maria Casapu [a] and
Jan-Dierk Grunwaldt ★[ab]

Iron exchanged zeolite catalysts have been synthesized by an aqueous ion-exchange using iron powder and acetic acid under a protective atmosphere. This simplified strategy for producing Fe(II) species *in situ* was found to lead to highly dispersed iron even within the zeolite framework of small-pore zeolites, which is attractive for various catalytic applications. The obtained samples were used for the selective catalytic reduction of NO_x with NH_3.

Zeolite-based catalysts are widely applied for numerous processes due to their high activity and selectivity combined with good hydrothermal stability.[1–5] Especially catalysts with incorporated transition metals like iron show excellent catalytic activity for oxidative cleavage,[6] N_2O decomposition[7–9] and selective catalytic reduction of NO_x[3,10–13] while being relatively low-cost materials.

Preparation of Fe-zeolites is typically achieved by traditional ion exchange and impregnation methods.[14] While the latter often results in high ratios of larger Fe oligomers and Fe_2O_3 particles with low crystallinity, the former has limited controllability. Particularly, partial oxidation of Fe^{2+} to Fe^{3+} species by atmospheric oxygen occurs during both methods, which promotes the formation of oligomeric species and clusters. Especially for small pore size zeolite frameworks like SSZ-13, such Fe^{3+}-clusters are typically larger than the available pores, resulting in poor ion exchange rates and a higher extent of Fe_2O_3 particle formation.[15] Furthermore, sources of Fe^{2+} for traditional ion exchange are limited due to the air-sensitive nature of Fe^{2+} salts. Commonly used salts like $FeSO_4$ additionally insert the SO_4^{2-} ions, which cannot be completely removed from the synthesized catalyst. Also, the addition of mild

reductant to the reaction mixture to avoid Fe^{2+} oxidation[16] or solid-state ion exchange were suggested.[17] Since monomeric $[Fe–(OH)_2]^+$ and dimeric $[HO–Fe–O–Fe–OH]^{2+}$ sites are assumed to be the active species for selective catalytic reduction (SCR) of NO, positioning of Fe at the ion exchange sites in the zeolite framework is preferred.[18,19] Therefore, tuning the preparation of Fe-zeolites to obtain a high ratio of monomeric/dimeric sites is crucial for achieving high catalytic activity. Recently, serval hydrothermal methods have been proposed that involve the introduction of the iron source together with the structure directing agent during the zeolite synthesis itself.[20–23] While these methods deliver the desired ion exchanged zeolite with a high degree of monomeric/dimeric Fe-sites, the inclusion of iron into the zeolite framework occurs as well to a certain extent during such synthetic approaches. Additionally, due to the usage of Fe-based structure directing agents the preparation method is limited to one specific zeolite morphology. As a substitute solution, an improved ion exchange method has been suggested by Long and Yang.[24] This method involves the generation of Fe^{2+} by dissolving Fe^0 in diluted HCl. However, already for low Fe loadings of 1.2 wt%[25] the formation of Fe_xO_y clusters was noticed. Furthermore, the use of corrosive HCl led to chlorine induced dealumination of the zeolite.[26] Hence, there is a need for a more facile method.

Herein, we describe an alternative method to synthesize Fe-exchanged zeolites that involves an improved ion exchange procedure. In this case, the *in situ* generation of Fe^{2+} ions is achieved by dissolving the Fe^0 powder in a degassed aqueous solution of acetic acid (CH_3COOH) under a protective argon atmosphere. The oxidation is initiated by heating the resulting mixture to elevated temperatures. Simultaneously with the formation of Fe^{2+} species, the ion exchange process is initiated. In this way, the further oxidation to Fe^{3+} and the growth of oligomers and clusters is circumvented. As a result of this approach, a fine distribution of Fe within the zeolite framework is achieved. To evaluate the outcome of the new preparation procedure in comparison with more conventional synthesis

a Institute for Chemical Technology and Polymer Chemistry (ITCP), Karlsruhe Institute of Technology (KIT), Karlsruhe, Germany

b Institute of Catalysis Research and Technology (IKFT), Karlsruhe Institute of Technology (KIT), Eggenstein-Leopoldshafen, Germany. E-mail: grunwaldt@kit.edu

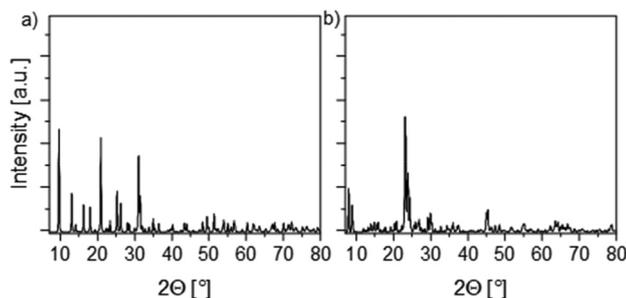† Electronic supplementary information (ESI) available. See DOI: https://doi.org/10.1039/d5cc02081f

Fig. 1 XRD patterns of Fe-SSZ-13 (a) and Fe-ZSM-5 (b) after synthesis.

approaches, additional catalyst samples were obtained using the conventional ion exchange method with $FeSO_4$ as precursor. The detailed synthesis procedures are summarized in the ESI.†

Two different zeolite frameworks (SSZ-13 and ZSM-5) were used to validate the transferability of this method. The XRD patterns obtained after the ion exchange process and calcination (Fig. 1) indicate the absence of iron oxide particles and confirm the intact structure of the zeolite frameworks.

The achieved iron loading as determined by inductively coupled plasma – optical emission spectrometry (ICP-OES) amounts to 1.4 wt% in the case of Fe-SSZ-13 and 2.6 wt% for Fe-ZSM-5 (Table 1). For the catalysts synthesized *via* the traditional ion exchange procedure, iron loadings of 1.0 wt% for Fe-SSZ-13 and 1.8 wt% for Fe-ZSM-5 were achieved (*cf.* Table S1, ESI†). As the concentration of Fe-ions in the solution and the exchange time were equal for both synthesis approaches, this result suggests a higher ion-exchange rate for the novel synthesis method. N_2-physisorption isotherms revealed that no loss occurred in the BET specific surface area[27] during the ion exchange with iron, which validates that the internal pores are not obstructed.

To further clarify the location and nature of iron species within the zeolite framework after the ion exchange procedure, the as prepared and calcined catalysts were characterized by UV-vis spectroscopy. A strong absorption band with a maximum at 264 nm was observed for Fe-SSZ-13 that can be attributed to the UV-absorption at octahedral Fe-sites.[19,25] The shoulder at 215 nm further indicates the presence of tetrahedral Fe-sites while the tail at 312 nm shows the presence of only a small amount of oligomeric sites. The absence of an absorption band at 550 nm further proves the non-existence of bulk Fe_xO_y species on the external surface of the zeolite.[28]

For Fe-ZSM-5 the absorption bands for tetrahedral (217 nm) and octahedral Fe-sites (272 nm) were slightly shifted to higher wavelengths. The characteristic feature for Fe-oligomers was
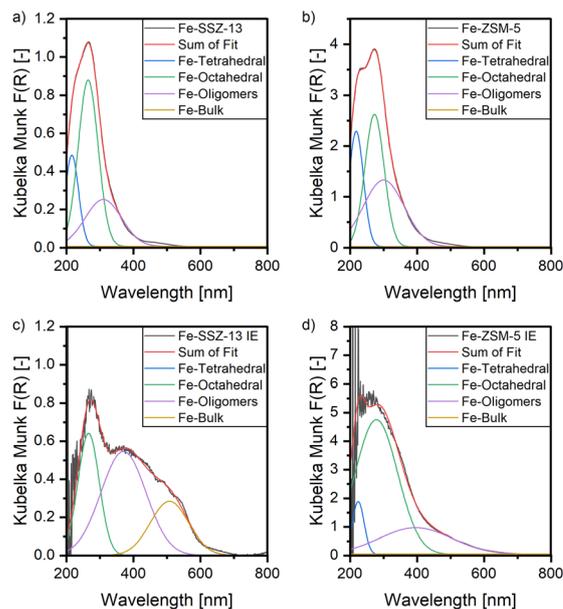

Fig. 2 UV-vis spectra of Fe-SSZ-13 (a) and Fe-ZSM-5 (b) catalyst prepared *via* improved ion-exchange and their Gauss fit to identify the nature of active sites.

centered around 304 nm, at slightly lower wavelength. In addition, no absorption of bulk Fe_xO_y could be detected.

The UV-vis spectrum obtained for the Fe-ZSM-5 sample synthesized by traditional ion exchange with $FeSO_4$ (Fig. 2c and d) shows similar absorption bands at 217 nm, 272 nm and 304 nm, with the band at 272 nm showing a higher contribution. This latter one suggests a higher concentration of Fe sites in octahedral coordination but a comparable coordination environment as observed for the Fe-SSZ-13 sample.

Conversely, for the Fe-SSZ-13 catalyst synthesized by traditional ion exchange a broad absorption band at 304 nm can be observed accompanied by a band at 550 nm. These indicate that the iron is primarily present as oligomeric species and small Fe_xO_y agglomerates. The relative amounts of the different iron species derived based on the UV-Vis data are summarized in Table S2 (ESI†).

The as prepared catalysts were further characterized by X-ray absorption spectroscopy (Fig. 3). In the X-ray absorption near edge structure (XANES) region, a pre-edge feature at 7114.5 eV and two white line features at 7132.7 eV and 7137.2 eV were visible for both samples. A slightly higher intensity could be observed for Fe-SSZ-13 but otherwise no further differences could be detected, suggesting similar coordination environments of Fe-ions in both catalysts. Based on the pre-edge feature at 7114.5 eV, complete oxidation to Fe^{3+} can be assumed.[29,30] The similarity of the pre-edge intensity and the white line position with those measured for the Fe_2O_3 reference (Fig. S1a, ESI†) suggests that a mixture of octahedrally and tetrahedrally coordinated Fe^{3+} sites were present in the zeolite-based samples, as already uncovered by UV-vis spectroscopy measurements (Fig. 2). In the FT-EXAFS data acquired for the two catalysts (Fig. 3b), a first coordination shell is visible
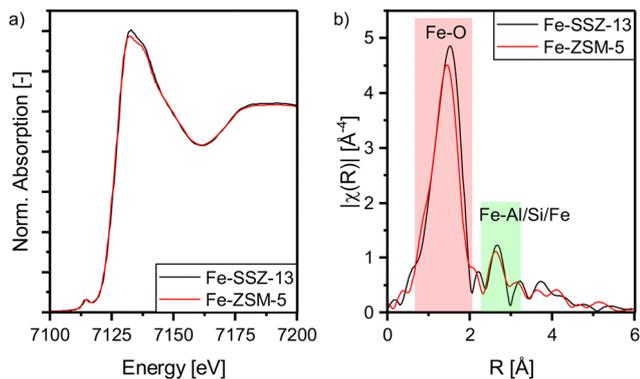
Table 1 Achieved metal loading determined by ICP-OES and internal surface area determined by N_2-physisortion using BET isotherm

Sample	Fe-loading (wt%)	Si/Al ratio	S_{BET} (m² g⁻¹)
Fe-SSZ-13	1.4	14	784
Fe-ZSM-5	2.6	13	380

ChemComm

Communication

Fig. 3 Fe K-edge XANES spectra (a) and Fourier transformed k^3-weighted, phase uncorrected EXAFS spectra (b) of as prepared Fe-SSZ-13 (black) and Fe-ZSM-5 (red).

Fig. 5 Conversion of NH_3 (black line) and NO_x (red line) during NH_3-SCR over Fe-SSZ-13 synthesized by improved and traditional ion exchange. Gas composition: 350 ppm NO, 350 ppm NH_3, 12% H_2O, 10% O_2 in N_2.

around 1.5 Å (not corrected for the phase-shift) that can be associated to the oxygen atoms of the zeolite framework. The observed distance of the Fe–O scattering path is similar to that obtained for the Fe_2O_3 reference samples (Fig. S1b, ESI†), which confirms the presence of Fe^{3+} species in these samples. A second coordination shell with low intensity could be observed at 2.6 Å, and was attributed to another Fe or framework Si/Al atoms.[25,31]

Supplementary catalytic activity tests for NH_3 oxidation were conducted for both synthesized catalysts (Fig. S2, ESI†). No NH_3 conversion below 350 °C and only a slight increase in activity was observed for both samples above 350 °C. Since larger clusters and Fe_xO_y particles are known to be more active for NH_3 oxidation than Fe monomers,[32] these results provide further evidence of the good distribution of Fe at ion-exchange positions.

The catalytic activity for the SCR of NO_x with NH_3 was investigated for both catalysts prepared by the improved as well as traditional ion exchange method (Fig. 5 and Fig. 4). A steady increase in the NO conversion could be observed above 250 °C for all investigated systems. Fe-ZSM-5 samples reached
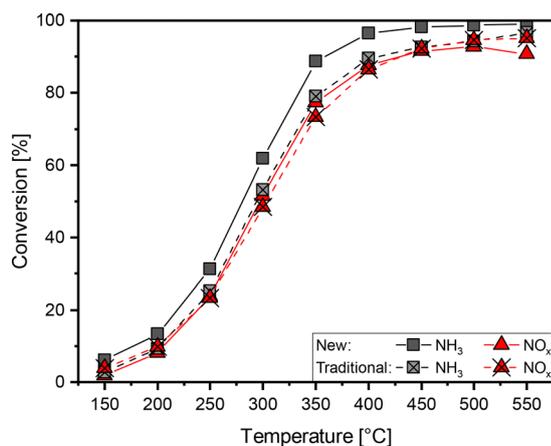
almost full conversion at 350 °C, independent of the synthesis method (Fig. 4). Nonetheless, a slightly lower performance was exhibited at all investigated temperatures by the catalysts obtained *via* the conventional ion exchange procedure. For both Fe-SSZ-13 catalysts, on the other hand, a high NO removal activity ($>60\%$) was measured only above 400 °C (Fig. 5). However, also in this case, the sample prepared by the improved ion exchange method showed a higher NO_x conversion up to 500 °C. Only at 550° both Fe-SSZ-13 samples displayed complete NO_x removal.

In a next step, the catalysts synthesized by the improved ion exchange method were hydrothermally aged at 650 °C and then tested for their SCR activity (*cf.* Fig. 6). In both cases, about 40% NO_x conversion was measured at around 300 °C with a maximum of about 80% observed at 550 °C. This trend indicates a decrease in the overall SCR performance for both catalysts

Fig. 4 Conversion of NH_3 (black line) and NO_x (red line) during NH_3-SCR over Fe-ZSM-5 synthesized by improved and traditional ion exchange. Gas composition: 350 ppm NO, 350 ppm NH_3, 12% H_2O, 10% O_2 in N_2.
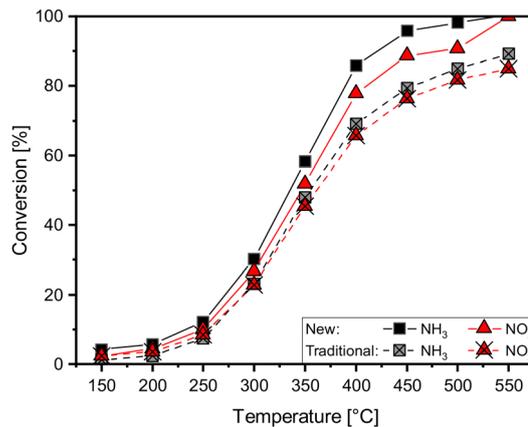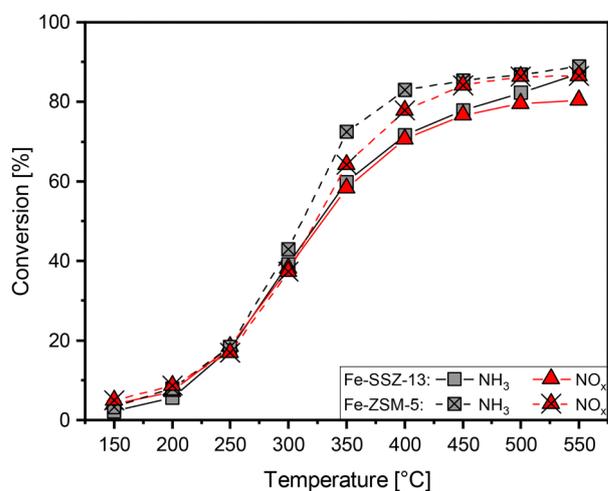

Fig. 6 Conversion of NH_3 (black line) and NO_x (red line) during NH_3-SCR over Fe-ZSM-5 (dashed lines) and Fe-SSZ-13 (solid lines) synthesized by improved ion exchange after hydrothermal aging (10% H_2O, 10% O_2 in N_2) at 650 °C for 16 h. Gas composition: 350 ppm NO, 350 ppm NH_3, 12% H_2O, 10% O_2 in N_2.

investigated, which is in line with the outcome of previous ageing studies for analogous Fe-zeolite systems.[33–35] By comparing the activity of the aged Fe-SSZ-13 with that of the fresh counterpart, a slight increase in the low temperature NO_x conversion ($<350\ °C$) is noticed. This behavior has previously been reported,[36] and has been assigned to a higher contribution of NO oxidation to NO_2 upon hydrothermal ageing. Ultimately, this leads to a more significant impact of the fast-SCR pathway on the overall NO_x conversion.

In conclusion, the successful synthesis of highly dispersed iron species (monomeric, dimeric) even in small-pore zeolites by an improved and more facile ion-exchange method was reported. By using the *in situ* and controlled oxidation of Fe^0 to Fe^{2+}, highly distributed Fe species were formed within the zeolite framework without detectable Fe_xO_y cluster formation even in small pore zeolites like SSZ-13. While the formation of small oligomeric species was observed by UV-vis spectroscopy, the absence of large Fe-clusters is illustrated by the low levels of NH_3 overoxidation potential during NH_3-SCR of NO_x. Overall, these results validate the potential of the novel synthetic route for Fe-zeolites, which can as well be used for the preparation of mixed Cu-Fe-exchanged zeolites in the future. Furthermore, the obtained catalysts represent ideal candidates for future mechanistic studies to derive structure–activity correlations for the selective catalytic reduction of NO_x with NH_3.

Conflicts of interest

There are no conflicts to declare.

Data availability

Data for this article, including raw data are available at KITopen at [**https://doi.org/10.35097/2md98bz5tqda65ku**]. The data supporting this article have been included as part of the ESI.†

Notes and references

1 T. Ryu, Y. Kang, I.-S. Nam and S. B. Hong, *React. Chem. Eng.*, 2019, **4**, 1050–1058.
2 F. Gao, Y. Wang, M. Kollár, N. M. Washton, J. Szanyi and C. H. Peden, *Catal. Today*, 2015, **258**, 347–358.
3 M. Colombo, I. Nova and E. Tronconi, *Catal. Today*, 2010, **151**, 223–230.
4 T. J. Toops, K. Nguyen, A. L. Foster, B. G. Bunting, N. A. Ottinger, J. A. Pihl, E. W. Hagaman and J. Jiao, *Catal. Today*, 2010, **151**, 257–265.
5 S. Shwan, R. Nedyalkova, J. Jansson, J. Korsgren, L. Olsson and M. Skoglundh, *Ind. Eng. Chem. Res.*, 2012, **51**, 12762–12772.
6 P. Treu, B. B. Sarma, J.-D. Grunwaldt and E. Saraçi, *ChemCatChem*, 2022, **14**, e202200993.
7 K. Jíša, J. Nováková, M. Schwarze, A. Vondrová, S. Sklenák and Z. Sobalik, *J. Catal.*, 2009, **262**, 27–34.
8 J. Pieterse, S. Booneveld and R. van den Brink, *Appl. Catal., B*, 2004, **51**, 215–228.
9 M. L. Bols, B. E. Snyder, H. M. Rhoda, P. Cnudde, G. Fayad, R. A. Schoonheydt, V. Van Speybroeck, E. I. Solomon and B. F. Sels, *Nat. Catal.*, 2021, **4**, 332–340.
10 H.-Y. Chen, X. Wang and W. M. Sachtler, *Appl. Catal., A*, 2000, **194**, 159–168.
11 A. Grossale, I. Nova and E. Tronconi, *Catal. Today*, 2008, **136**, 18–27.
12 T. J. Toops, J. A. Pihl and W. P. Partridge, *Urea-SCR technology for deNOx after treatment of diesel exhausts*, 2014, 97–121.
13 R. Nedyalkova, S. Shwan, M. Skoglundh and L. Olsson, *Appl. Catal., B*, 2013, **138–139**, 373–380.
14 J. Zhang, X. Tang, H. Yi, Q. Yu, Y. Zhang, J. Wei and Y. Yuan, *Appl. Catal., A*, 2022, **630**, 118467.
15 F. Gao, Y. Zheng, R. K. Kukkadapu, Y. Wang, E. D. Walter, B. Schwenzer, J. Szanyi and C. H. Peden, *ACS Catal.*, 2016, **6**, 2939–2954.
16 A. Oda, K. Aono, N. Murata, K. Murata, M. Yasumoto, N. Tsunoji, K. Sawabe and A. Satsuma, *Catal. Sci. Technol.*, 2022, **12**, 542–550.
17 F. Martinovic, S. Ballauri, N. Blangetti, S. Bensaid, R. Pirone, B. Bonelli, M. Armandi and F. A. Deorsola, *Appl. Catal., A*, 2023, **658**, 119160.
18 R. Zhang, E. Anderst, K. Groden and J.-S. McEwen, *Ind. Eng. Chem. Res.*, 2018, **57**, 13396–13405.
19 M. Høj, M. J. Beier, J.-D. Grunwaldt and S. Dahl, *Appl. Catal., B*, 2009, **93**, 166–176.
20 M. L. Bols, J. Devos, H. M. Rhoda, D. Plessers, E. I. Solomon, R. A. Schoonheydt, B. F. Sels and M. Dusselier, *J. Am. Chem. Soc.*, 2021, **143**, 16243–16255.
21 S. Zhang, P.-S. Li, J.-X. Zhang, Y.-H. Qin, Z. Chen, L. Yang, T. Wang and C.-W. Wang, *Fuel*, 2025, **394**, 135117.
22 J. Li, S. Ma, K. Ren and N. Xu, *Mol. Catal.*, 2023, **537**, 112920.
23 K. Niu, G. Li, J. Liu and Y. Wei, *J. Solid State Chem.*, 2020, **287**, 121330.
24 R. Long and R. T. Yang, *Catal. Lett.*, 2001, **74**, 201–205.
25 M. Schwidder, M. S. Kumar, K. Klementiev, M. M. Pohl, A. Brückner and W. Grünert, *J. Catal.*, 2005, **231**, 314–330.
26 P. Kern, M. Klimczak, T. Heinzelmann, M. Lucas and P. Claus, *Appl. Catal., B*, 2010, **95**, 48–56.
27 S. Brunauer, P. H. Emmett and E. Teller, *J. Am. Chem. Soc.*, 1938, **60**, 309–319.
28 L. Čapek, V. Kreibich, J. Dědeček, T. Grygar, B. Wichterlova, Z. Sobalik, J. Martens, R. Brosius and V. Tokarova, *Microporous Mesoporous Mater.*, 2005, **80**, 279–289.
29 A. Boubnov, H. Lichtenberg, S. Mangold and J.-D. Grunwaldt, *J. Synchrotron Radiat.*, 2015, **22**, 410–426.
30 P.-E. Petit, F. Farges, M. Wilke and V. A. Solé, *J. Synchrotron Radiat.*, 2001, **8**, 952–954.
31 A. Battiston, J. Bitter, W. Heijboer, F. De Groot and D. Koningsberger, *J. Catal.*, 2003, **215**, 279–293.
32 S. Campisi, S. Palliggiano, A. Gervasini and C. Evangelisti, *J. Phys. Chem. C*, 2019, **123**, 11723–11733.
33 L. Kovarik, N. M. Washton, R. Kukkadapu, A. Devaraj, A. Wang, Y. Wang, J. Szanyi, C. H. Peden and F. Gao, *ACS Catal.*, 2017, **7**, 2458–2470.
34 X. Tan, P. García-Aznar, G. Sastre and S. B. Hong, *J. Am. Chem. Soc.*, 2024, **146**, 6352–6359.
35 S. Brandenberger, O. Kröcher, M. Casapu, A. Tissler and R. Althoff, *Appl. Catal., B*, 2011, **101**, 649–659.
36 F. Gao, J. Szanyi, Y. Wang, B. Schwenzer, M. Kollár and C. H. Peden, *Top. Catal.*, 2016, **59**, 882–886.